

Support Information

Double-walled heterostructured $\text{Cu}_{2-x}\text{Se}/\text{Cu}_7\text{S}_4$ nanoboxes with enhanced electrocatalytic activity for quantum dot sensitized solar cells

*Lei Ran, Longwei Yin**

*Key Laboratory for Liquid-Solid Structural Evolution and Processing of Materials,
Ministry of Education, School of Materials Science and Engineering, Shandong
University, Jinan 250061, P.R. China*

**To whom correspondence should be addressed. Tel.: + 86 531 88396970. Fax: + 86*

531

88396970. E-mail: yinlw@sdu.edu.cn

Supplementary procedures for Experiments details:

Materials

The chemicals used in this work were copper sulfate pentahydrate ($\text{CuSO}_4 \cdot 5\text{H}_2\text{O}$), sodium hydroxide (NaOH), sodium citrate, ascorbic acid, sodium sulfide nonahydrate ($\text{Na}_2\text{S} \cdot 9\text{H}_2\text{O}$), selenium powder (Se), ammonium hydroxide ($\text{NH}_3 \cdot \text{H}_2\text{O}$), sodium borohydride (NaBH_4), Cu foil, hydrochloric acid (HCl), chloroplatinic acid (H_2PtCl_6), butyl alcohol, tetrabutyl titanate, boric acid, cadmium acetate dihydrate ($(\text{CH}_3\text{COO})_2\text{Cd} \cdot 2\text{H}_2\text{O}$), cadmium sulfate ($\text{CdSO}_4 \cdot 8/3\text{H}_2\text{O}$), sodium bisulfite (Na_2SO_3), nitrilotriacetic acid trisodium salt monohydrate ($\text{N}(\text{CH}_2\text{COONa}) \cdot 3\text{H}_2\text{O}$), zinc nitrate hexahydrate ($\text{Zn}(\text{NO}_3)_2 \cdot 6\text{H}_2\text{O}$), sublimed sulfur (S), potassium chloride (KCl), TiO_2 (Degussa P25), terpineol, ethyl cellulose (EC), anhydrous ethanol. All chemical reagents in the experiments were analytical pure and used without any further treatment.

Synthesis of solid Cu_2O nanocube

The Cu_2O nanocubes were synthesized by a method according to the previous report.¹ 0.3745 g $\text{CuSO}_4 \cdot 5\text{H}_2\text{O}$ was dissolved into 100 ml deionized water under magnetic stirring at room temperature, followed by the addition of 0.15 g sodium citrate and 1.0 g NaOH , stirring for two minutes. Then, 0.264 g ascorbic acid was dissolved into 50 ml deionized water and added to above mixture. After an hour, the precipitates were collected by centrifugation and washed with deionized water.

Synthesis of 300nm scattering TiO_2 particles

The synthesis of 300nm scattering TiO_2 particles can be synthesized by a method according to the previous report.² 3.4 mL of tetrabutyl titanate and 25.5 mL of butyl alcohol were mixed to form a clear solution. The transparent mixture was added slowly into 100 mL of a 0.85M boric acid solution. After aging for 72 h at room temperature, the resultant precipitate was purified by centrifugation, washed with deionized water and ethanol, and dried in a vacuum oven. Finally, the powder was annealed at 450 °C and maintained at this temperature for 3 h.

Preparation of CEs based on DW- $\text{Cu}_{2-x}\text{Se}/\text{Cu}_7\text{S}_4$ -HNBs, SW- Cu_7S_4 -NBs

The SW- Cu_7S_4 -NBs and DW- $\text{Cu}_{2-x}\text{Se}/\text{Cu}_7\text{S}_4$ -HNBs were deposited on FTO by using a spin coating technique.³ More specifically, 0.10g of the prepared DW- $\text{Cu}_{2-x}\text{Se}/\text{Cu}_7\text{S}_4$ -HNBs or SW-

Cu₇S₄-NBs was added to the mixture of 0.5g terpineol and 1.0g of 10 wt% ethyl cellulose ethanol solution followed by continuous sonication for 30 min to get a homogeneous paste. The as-prepared pastes were spin-coated onto the drilled and cleaned (thoroughly washed by scrubbing, and followed with acetone, ethanol and deionized water under sonication for 30 min, respectively) FTO glass followed by annealing at 450°C in Ar atmosphere for 30 min.

Supplementary analysis for Results and discussion

Structure and morphology of SW-Cu₇S₄-NBs and DW-Cu_{2-x}Se/Cu₇S₄-HNBs

The XRD results shown in Fig.S1(d) suggests that the pure monoclinic Cu₇S₄ nanoboxes can be obtained through the sulfidation process and the consequent dissolution process of incipient Cu₂O templates, which follows the analogous mechanism except the vacancy of Se²⁻ precursor as mentioned in manuscript.

Fig.S3 (a) obviously reveals that the Cu₂O templates are composed of nearly dispersive nanocubes, which not only have a uniform size with an edge length of about 1 μm, but also has smooth surfaces, which is consistent with previous reports. Fig.S3(b-c) show the low-magnification FESEM images of the SW-Cu₇S₄-NBs, in which Cu₇S₄ nanoboxes have a size of about 1 μm and cubic morphology similar to that of Cu₂O nanocubes. Some partially broken nanoboxes can also be observed in Fig. S3 (b), implying that nanoboxes with hollow interiors are synthesized. As shown in Fig.S3 (d), the hollow structure of the obtained Cu₇S₄ nanobox is clearly further revealed on the individual broken nanobox.

The EDS spectrum and elemental mapping in Fig.S5 illustrates the SW-Cu₇S₄-NBs are composed of Cu and S elements, which are homogeneously distributed in SW-Cu₇S₄-NBs.

The TEM images and SAED shown in Fig .S6 indicate the Cu₇S₄ nanoboxes are made of rough cubic shell with voids inside and revealing the porous structures and the hollow nature. Typical TEM image in Fig.S6(b) shows that the edge length is about 1 μm and the thickness of shell is about 80 nm, which is consistent with the foregoing SEM analysis. HRTEM image in Fig.S6(c) indicates Cu₇S₄ nanobox is composed of fine nanoparticles and shows high crystallinity. The clear interplanar spacing of 0.300 nm corresponds well to the distance of (804) lattice plane. As displayed in Fig. S6(d), the corresponding SAED pattern shows the single crystal nature of as-synthesized SW-Cu₇S₄-NBs. The diffraction spots in Fig.S6(d) correspond well with those of the (886), (886), (0 16 0) planes of monoclinic Cu₇S₄ phase.

As indicated in Fig.S8 (a), only the peaks of C, O, Cu and S are observed in the XPS surveys of SW-Cu₇S₄-NBs, and no other evident impurities were detected in the sample. The ratio of Cu and S obtained from XPS results is 7.00: 3.86, which tallies well with the stoichiometric Cu₇S₄. Fig.S8 (b-c) display the high resolution XPS spectra of Cu 2p and S 2p from Cu₇S₄ nanoboxes. As can be seen from the XPS spectra of Cu2p orbit in Fig.S8(b), two main peaks located at 932.3 and 952.2 eV correspond to Cu2p_{3/2} and Cu2p_{1/2} respectively, which is proved existence of Cu⁺ in the Cu₇S₄ nanoboxes. And the two peaks located at 934.7 and 954.5 eV can be fitted into Cu2p_{3/2} and Cu2p_{1/2} respectively, which is proved existence of Cu²⁺ in the Cu₇S₄ nanoboxes. **The spectrum also exhibited another two satellite peaks at 943.4 and 962.0 eV, which is also reported in the previous work.** ⁴⁻⁶ Fig.S8 (c) shows the S2p XPS spectrum, which indicates the binding energies of 162.5 and 163.5 eV are attributed to S²⁻-coordinated to Cu⁺ and Cu²⁺ species in Cu₇S₄ nanoboxes. These values are close to the previous reported values, indicating the high purity of the Cu₇S₄ sample. **Similarly, the binding energy centered at around 167-169 eV (shown by arrows in Fig. S8c) matches with S-O bonding resulted from the oxidation effect.** ^{7,8}

The optical performance and photovoltaic properties of QDSSCs assembled by SW-Cu₇S₄-NBs, DW-Cu_{2-x}Se/Cu₇S₄-HNBs, Cu₂S/brass and Pt CEs

More specifically, the reference cell assembled by home-made Pt CE displays a J_{SC} of 20.70 mA·cm⁻², a V_{OC} of 0.407 V, and a FF of 18.32, yielding an PCE (η) of 1.54%, which is comparable to the previous reports. Compared to Pt based QDSSC, the device based on Cu₂S achieves a higher PCE (η) of 3.43% with an enhancement in J_{SC} of 21.72 mA·cm⁻², V_{OC} of 0.476 V and FF of 33.17, which has verified the potential application of copper chalcogenides in solar cells. Despite that Cu₂S has widely been recognized as the most effective CE for QDSSC, the stagnation in the photovoltaic performance due to sustaining damage of electrodes has prompted the development of novel CE catalysts with even higher catalytic activity and lower transfer resistance. The worst performance of Pt based QDSSC can be assigned to the “poisoning effect” at the interface of CE and electrolyte, which weakens the conductivity and catalytic activity of the CE material, and leads to a lower fill factor and power conversion efficiency.

The electrocatalytic performance of SW-Cu₇S₄-NBs, DW-Cu_{2-x}Se/Cu₇S₄-HNBs, Cu₂S/brass and Pt CEs

The bulk resistance of CE materials, the resistance of the FTO substrate and the contact resistance

jointly comprise the ohmic series resistance (R_S), which is tightly associated with the electrical conductivity. The R_{CT1} is generally investigated to interpret the contact state between the substrate and catalytic material films. The R_{CT2} is perceived as the pivotal parameter determining the catalytic activity of CE materials toward the reduction of S^{2-} and Sn^{2-} , exhibiting a contrary tendency compared with the catalytic activity of different CEs. As we expected, due to serious chemisorption of sulphur species on Pt CEs,⁹ all the parameters including R_S , R_{CT1} and R_{CT2} are larger than other CEs, resulting in their lowest catalytic activity and smallest PCE and further indicating higher catalytic activity of copper chalcogenides based CEs. Specifically, the smallest R_S of brass/ Cu_2S CE (27.73Ω) may be due to its brass-metal substrate, which has better conductivity than FTO substrate employed in other CEs. In spite of both the R_S and R_{CT1} of the brass/ Cu_2S CE (27.73Ω and 21.14Ω , respectively) are smaller than those of the SW- Cu_7S_4 -NBs CE and DW- $Cu_{2-x}Se/Cu_7S_4$ -HNBs CE, the larger R_{CT2} (4 times that of SW- Cu_7S_4 -NBs and 8 times that of DW- $Cu_{2-x}Se/Cu_7S_4$ -HNBs CE, respectively) slows the charge transfer process at the electrolyte-CE interface and ultimately limits its electrocatalytic activity and QDSSC performance. What's more, Pt CE possesses a larger charge transfer resistance (R_{CT2}) of 590.45Ω in comparison with Cu_2S CE (350.49Ω).

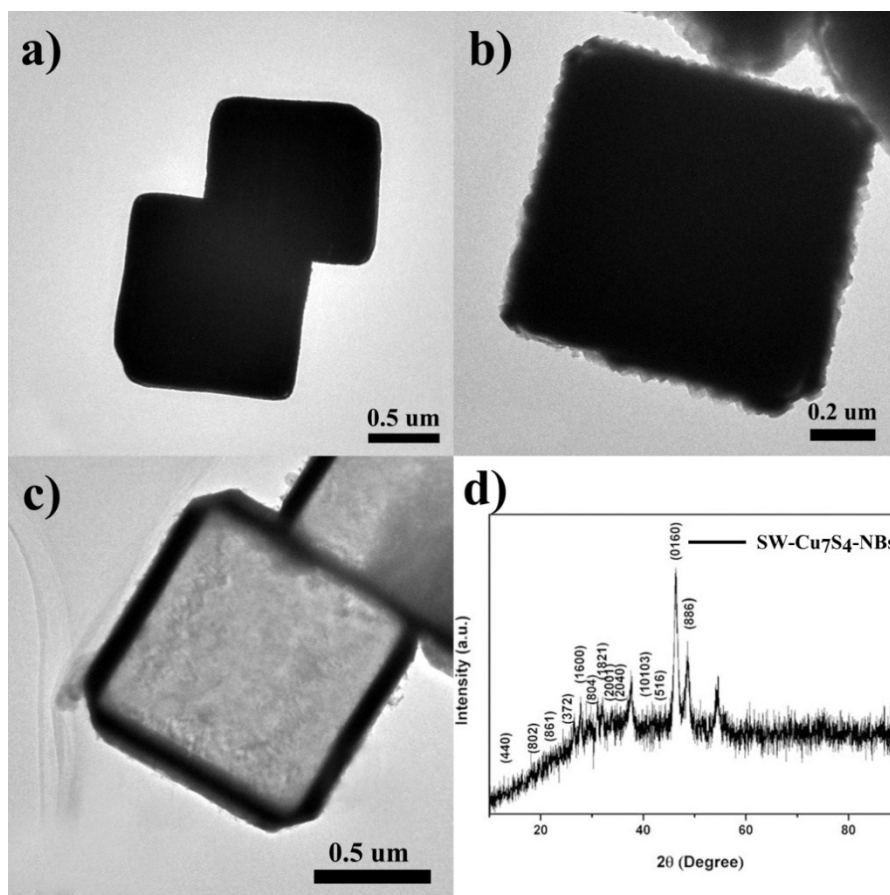


Fig.S1 (a-c) TEM and (d) XRD images of SW-Cu₇S₄-NBs obtained at different synthetic stage of entire process.

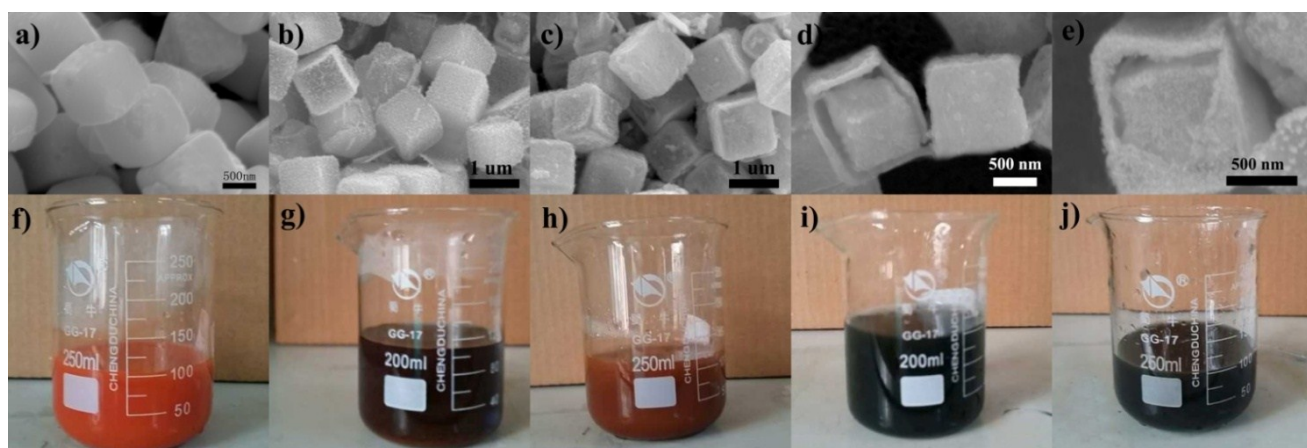


Fig.S2 (a-e) SEM images and (f-j) the digital photos of color variations of DW- Cu_{2-x}Se/Cu₇S₄-HNBs along the formation of intermediate products in synthesis process.

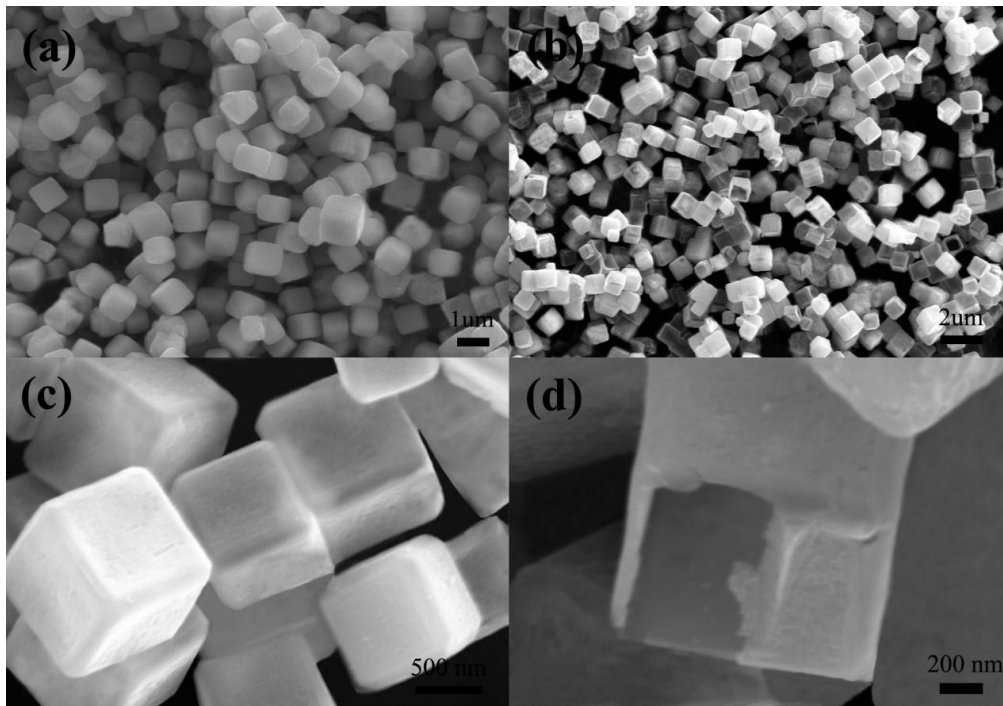


Fig.S3 FESEM images of the as-prepared SW-Cu₇S₄-NBs sample.

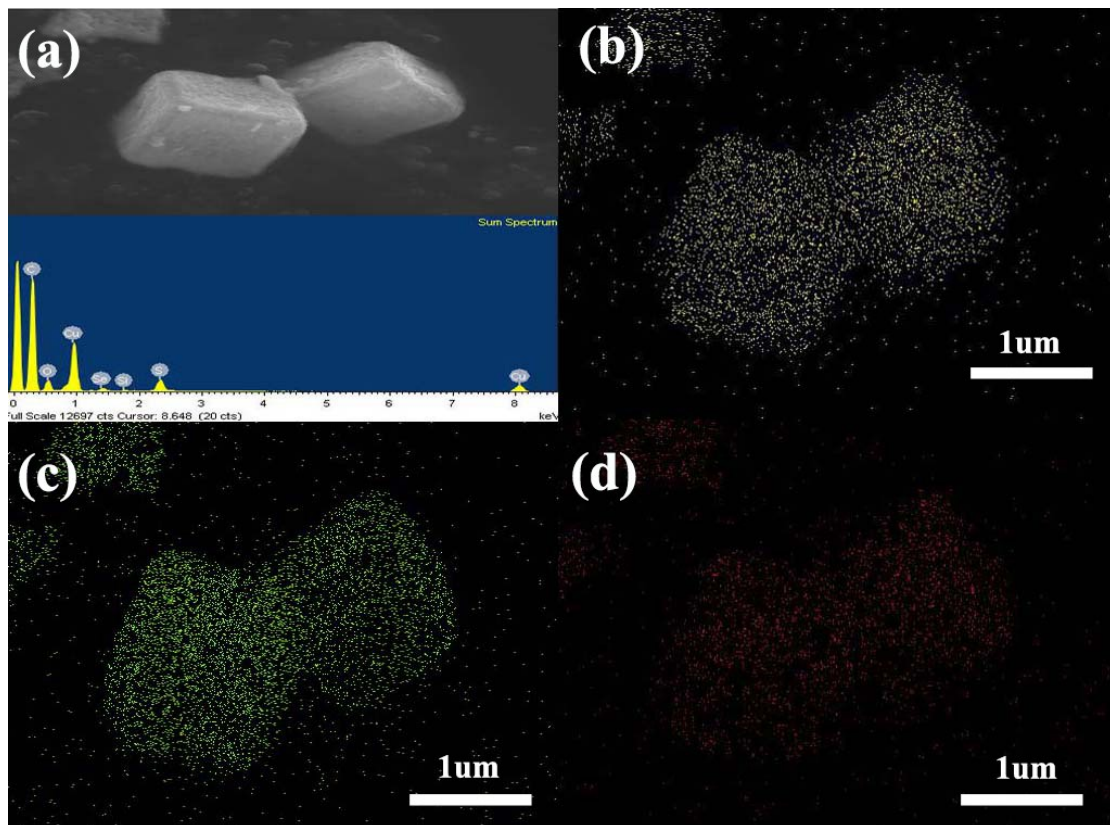


Fig.S4 (a) EDS spectrum and (b-d) elemental mapping of the as-prepared DW-Cu_{2-x}Se/Cu₇S₄-HNBs sample.

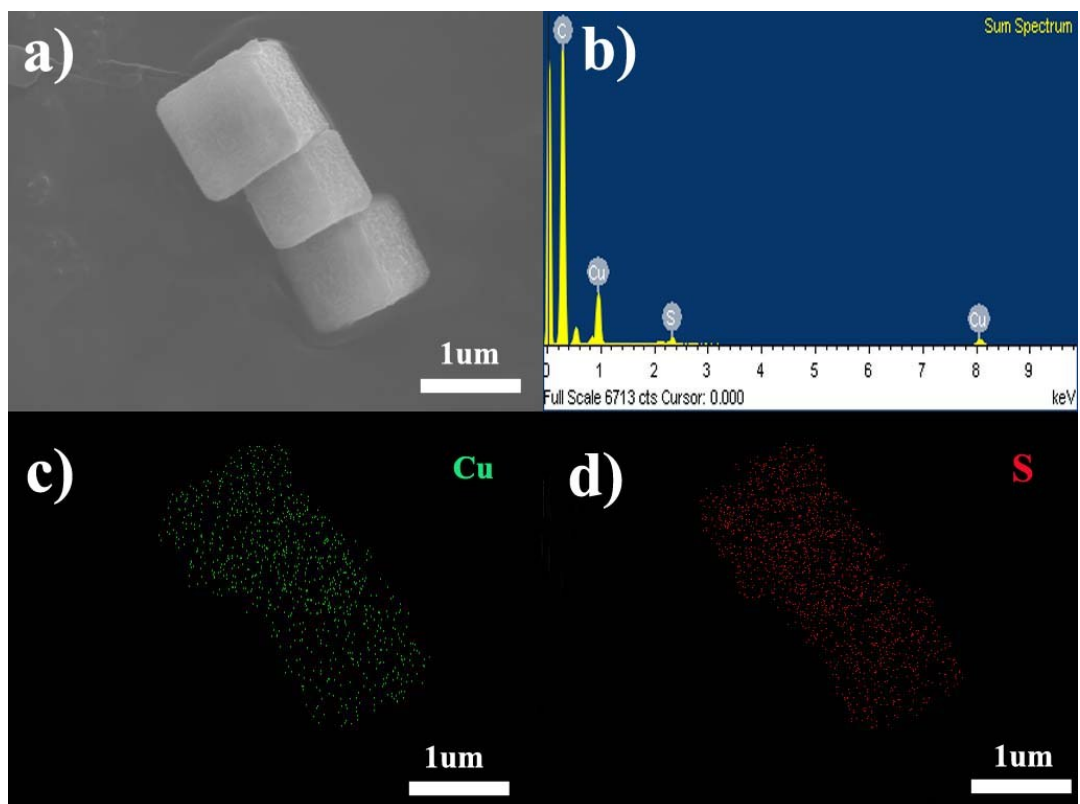


Fig.S5 (a) EDS spectrum and (b-d) elemental mapping of the as-prepared SW-Cu₇S₄-NBs sample.

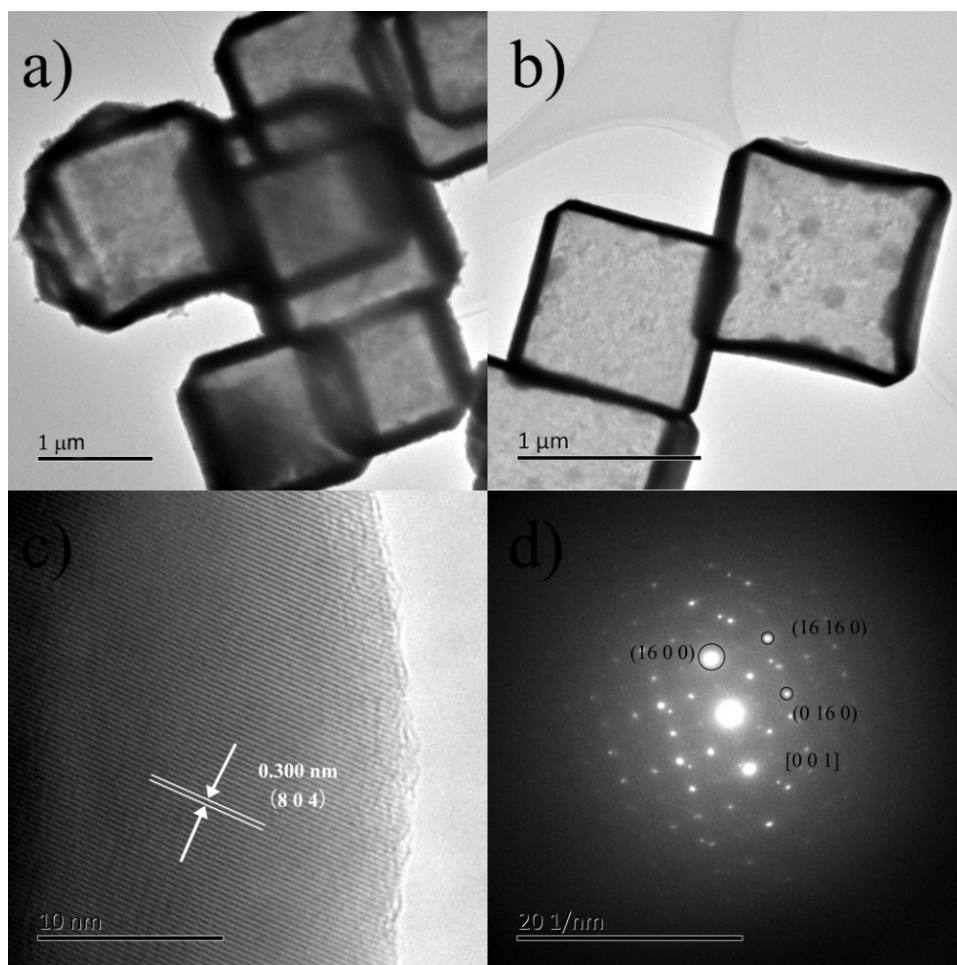


Fig.S6 (a-c) TEM images and (d) SAED pattern of the as-prepared SW-Cu₇S₄-NBs sample.

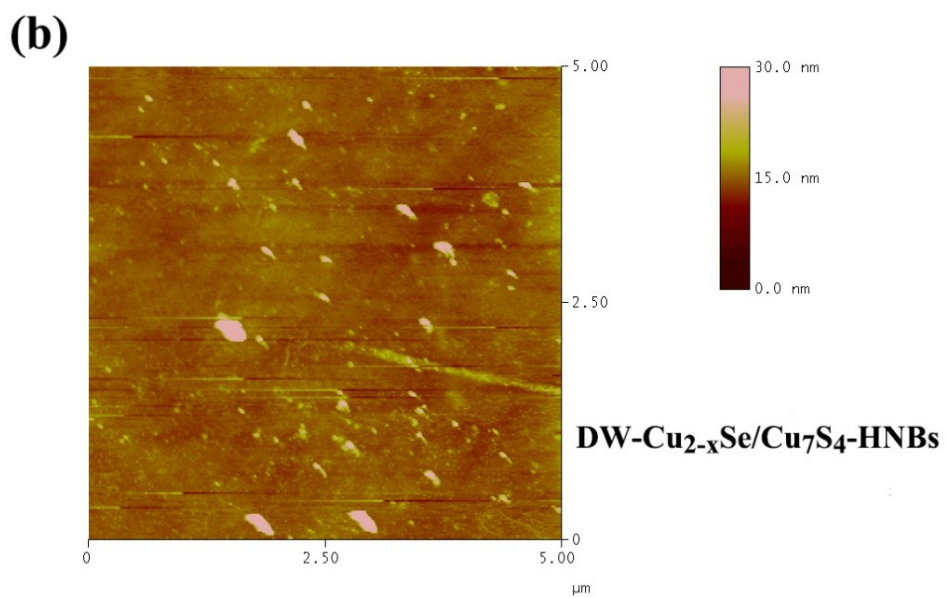
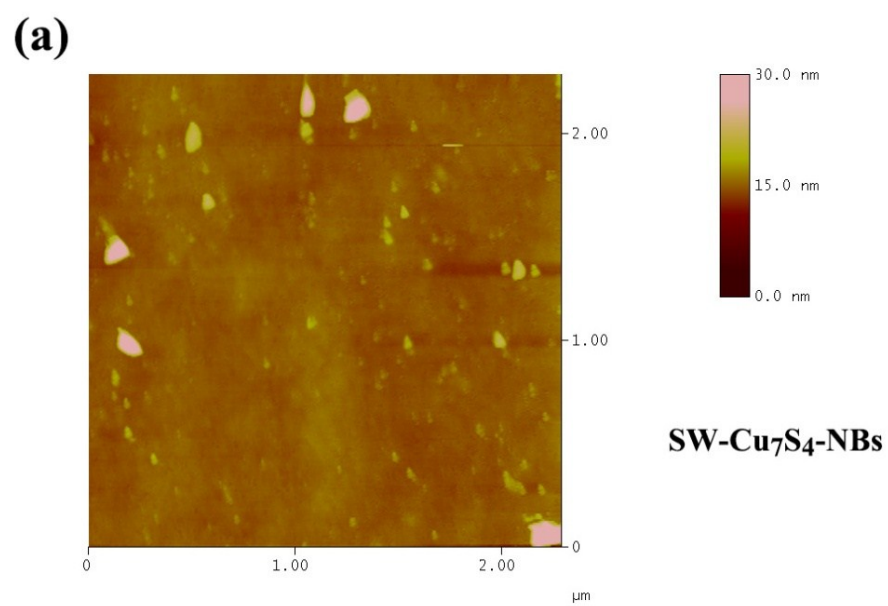


Fig.S7 AFM images of (a) SW-Cu₇S₄-NBs and (b) DW-Cu_{2-x}Se/Cu₇S₄-HNBs.

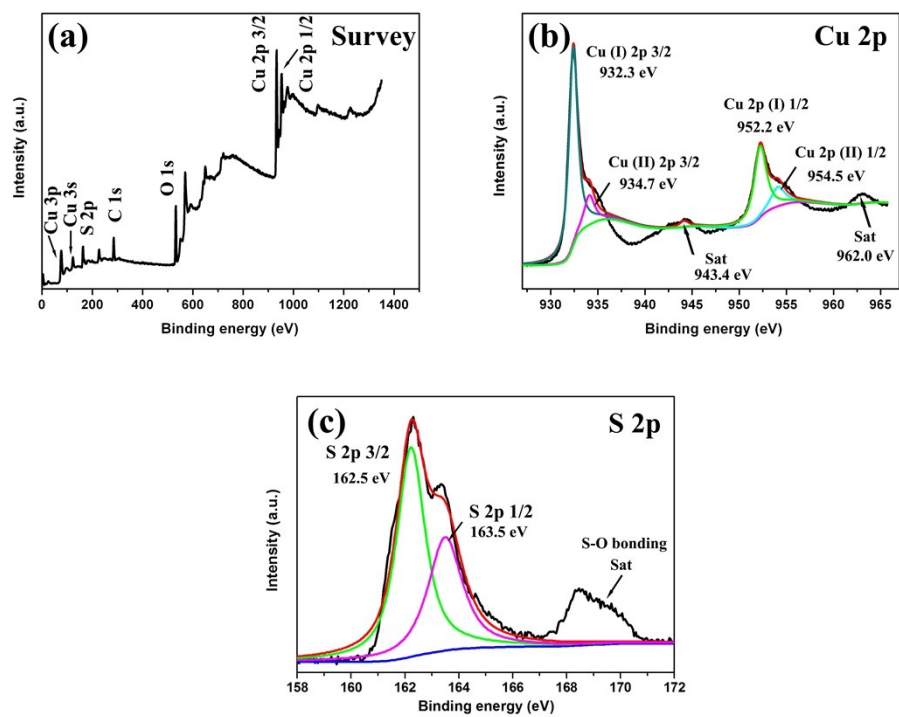


Fig.S8 XPS spectra of SW-Cu₇S₄-NBs sample. (a) Survey spectrum, (b) Cu 2p, (c) S2p.

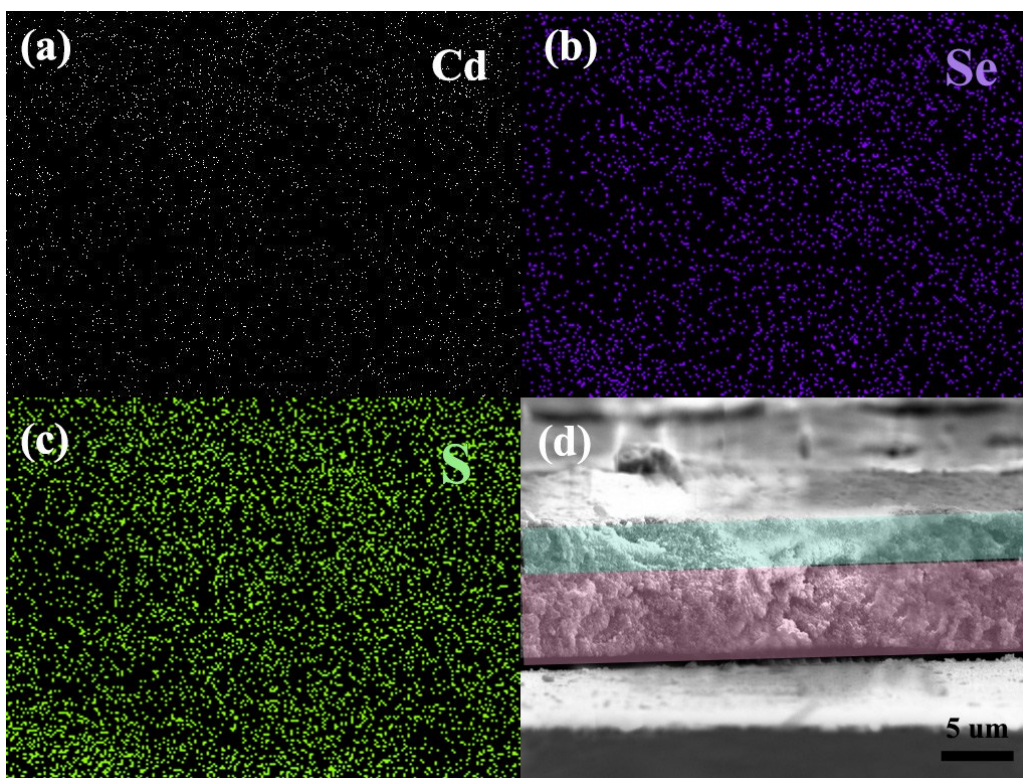


Fig.S9 (a-c) Elemental mapping of Cd, Se and S by EDS spectroscopy showing the uniform distribution of the CdSe/CdS QDs in the QDSSC device; (d) Cross-sectional SEM image of CdSe/CdS sensitized TiO₂ photoanode consisting of a 8 μm thick transparent layer and a 4 μm thick scattering layer.

Reference:

1. Cao, H.; Qian, X.; Zai, J.; Yin, J.; Zhu, Z., Conversion of Cu₂O nanocrystals into hollow Cu_{2-x}Se nanocages with the preservation of morphologies. *Chemical Communications* **2006**, 43 (43), 4548-4550.
2. Zhang, H.; Wang, C.; Peng, W.; Yang, C.; Zhong, X., Quantum dot sensitized solar cells with efficiency up to 8.7% based on heavily copper-deficient copper selenide counter electrode. *Nano Energy* **2016**, 23, 60-69.
3. Du, Z.; Zhang, H.; Bao, H.; Zhong, X., Optimization of TiO₂ photoanode films for highly efficient quantum dot-sensitized solar cells. *Journal of Materials Chemistry A* **2014**, 2 (32), 13033-13040.
4. Chusuei, C. C.; And, M. A. B.; Goodman, D. W., Correlation of Relative X-ray Photoelectron Spectroscopy Shake-up Intensity with CuO Particle Size. *Langmuir* **1999**, 15 (8).
5. Hsieh, S.; Lin, P. Y.; Chu, L. Y., Improved Performance of Solution-Phase Surface-Enhanced Raman Scattering at Ag/CuO Nanocomposite Surfaces. *Journal of Physical Chemistry C* **2014**, 118 (23), 12500-12505.

6. Hu, W.; Chen, R.; Xie, W.; Zou, L.; Qin, N.; Bao, D., CoNi₂S₄ Nanosheet Arrays Supported on Nickel Foams with Ultrahigh Capacitance for Aqueous Asymmetric Supercapacitor Applications. *Acs Applied Materials & Interfaces* **2014**, *6* (21), 19318.
7. Kung, M. L.; Tai, M. H.; Lin, P. Y.; Wu, D. C.; Wu, W. J.; Yeh, B. W.; Hung, H. S.; Kuo, C. H.; Chen, Y. W.; Hsieh, S. L., Silver decorated copper oxide (Ag@CuO) nanocomposite enhances ROS-mediated bacterial architecture collapse. *Colloids & Surfaces B Biointerfaces* **2017**, *155*, 399-407.
8. Wang, T.; Liu, M.; Ma, H., Facile Synthesis of Flower-Like Copper-Cobalt Sulfide as Binder-Free Faradaic Electrodes for Supercapacitors with Improved Electrochemical Properties. *Nanomaterials* **2017**, *7* (6), 140.
9. Lee, S. Y.; Park, M. A.; Kim, J. H.; Kim, H.; Choi, C. J.; Lee, D. K.; Ahn, K. S., Enhanced Electrocatalytic Activity of the Annealed Cu_{2-x}S Counter Electrode for Quantum Dot-Sensitized Solar Cells. *Journal of the Electrochemical Society* **2013**, *160* (11), H847-H851.